Plasma Chemistry and Plasma Processing, Vol. 22, No. 2, June 2002 (© 2002)

Electron Density and Energy Distributions in the Positive DC Corona: Interpretation for Corona-Enhanced Chemical Reactions

Junhong Chen[1] and Jane H. Davidson[1,2]

Received May 30, 2001; accepted September 10, 2001

Electrons produced in atmospheric pressure corona discharges are used for a variety of beneficial purposes including the destruction of gaseous contaminants, and surface treatment. In other applications, such as electrostatic precipitators and photocopiers, unintended reactions such as ozone production and deposition of silicon dioxide are detrimental. In both situations, a kinetic description of the electron distribution in the corona plasma is required to quantify the chemical processes. In this paper, the electron density and energy distributions are numerically determined for a positive dc corona discharge along a wire. The electron density distribution is obtained from the 1-D charge carrier continuity equations and Maxwell's equation. The non-Maxwellian electron kinetic energy distribution is determined from the Boltzmann equation. The effects of wire size (10-1000 μm) and current density (0.1–100 μA/cm of wire) on number density and energy distribution of electrons are presented. With increasing current, the electron density increases, but the thickness of the plasma and the electron energy distribution are not affected. Smaller electrodes produce thinner plasmas and fewer, but more energetic electrons, than larger wires. The effect of electrode size on the electron-impact chemical reaction rate is illustrated by the rates of dissociation and ionization of oxygen and nitrogen.

KEY WORDS: Corona discharge; electron density distribution; Boltzmann equation; electron energy distribution.

1. INTRODUCTION

Atmospheric pressure corona discharges have been used for decades to produce ions for charging surfaces or particles in photocopiers, electrostatic precipitators, and jet printers. In these applications, the useful ions are those that drift outside the corona ionization region. More recently, interest has turned toward using the corona discharge to drive chemical reactions, for example to decompose gaseous pollutants (e.g., NO_x, SO_2, and volatile organics)[1–8] or to produce desirable surface characteristics in polymer films

[1]Department of Mechanical Engineering, University of Minnesota, Minneapolis, MN 55455.
[2]To whom all correspondence should be addressed.

0272-4324/02/0600-0199/0 © 2002 Plenum Publishing Corporation

and fabrics.[9,10] These applications rely on energetic electrons in the corona plasma. Of course, unintended reactions can occur in any device in which a corona is present. For example, it is well known that ozone is produced in electrostatic precipitators and photocopiers.[11–16] In addition, if contaminant vapors, such as silicone, are present in the air stream, these species may react with electrons in a complex chain of reactions to produce a solid film on the high-voltage discharge electrode.[17–23] This process is similar to the plasma-enhanced chemical vapor deposition (PECVD) used in the semiconductor industry.

Desirable or not, the electron-impact chemical reaction rate depends on the density and the kinetic energy of the electrons in the corona plasma. Although chemical processes in low-pressure plasmas have received a great deal of attention,[24–28] little is known about either the energy distribution of electrons or chemical reaction rates in corona plasmas. Most of the prior analytical and numerical work has focused on characterizing the electric field and current distributions in the unipolar ionic drift region outside the active ionization region. The distribution of ionic species and electrons in the corona plasma have been modeled,[29,30] but the diffusion of electrons was neglected. The energy distribution of electrons has not been determined.

In this paper, the electron density and kinetic energy distributions for a direct current (dc) uniform, positive-polarity wire discharge in dry air at atmospheric pressure are determined. The electron density distribution is obtained by solving the continuity equations following Townsend avalanche theory and Maxwell's equation. The electron kinetic energy distribution is determined by solving the spatially homogeneous Boltzmann equation. Because the current density and the electrode diameter control the electron distribution, these parameters are varied to assess their effects on the number density and energy distribution of electrons within the plasma region. The rates of dissociation and ionization of O_2 and N_2 in the corona plasma are calculated based on above results to elucidate the effect of wire size.

2. PHYSICS OF THE POSITIVE CORONA DISCHARGE

The corona discharge is normally used at atmospheric pressure. Figure 1 illustrates the positive-polarity, direct current corona discharge in the coaxial wire-cylinder geometry. A high positive voltage is applied to the small diameter wire discharge electrode and the larger diameter cylinder is grounded. Free electrons formed naturally in the interelectrode space are accelerated toward the wire. In a region very near the wire, where the electric field strength is greater than 3×10^6 V/m, inelastic collisions of electrons and neutral gas molecules produce electron-positive ion pairs. In air, O_2^+ and N_2^+ dominate. The newly freed electrons are in turn accelerated by the

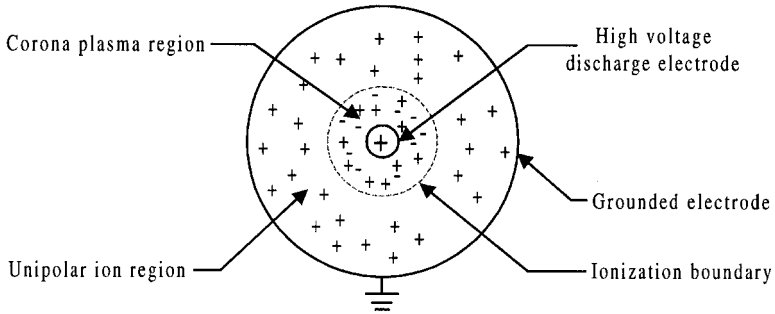

Fig. 1. Sketch of a positive dc corona discharge in a wire-cylinder electrode geometry. The dashed line indicates the outer boundary of the ionization region. Not to scale.

electric field and produce further ionization. Secondary electrons produced by photons emitted during the de-excitation process in the plasma region sustain the discharge. The ionization region is uniform along the wire surface and appears as a weak bluish glow. Negative coronas are non-uniform and the mechanisms for generation differ from those described for a positive corona.

Free electrons may also attach to electronegative gas molecules (for instance, O_2) to form negative ions or recombine with positive ions. Because the recombination coefficients are small[31] and the charge density is relatively low, recombination is usually negligible. Consequently, ionization competes primarily with electron attachment. Near the high-voltage wire, ionization prevails over attachment and new electrons are produced. A few wire diameters away, at the outer edge of the corona plasma, the ionization rate equals the attachment rate. All newly produced electrons attach to molecules to form negative ions. Beyond the corona plasma region, the field strength is inadequate to produce electrons. Unipolar ions of the same polarity as the discharge electrode drift into this volume toward the grounded cylinder. Positive ions are responsible for all current outside the active ionization region. Negative ions move toward the discharge electrode. Usually, ions do not have high enough energy to cause ionization. The grounded electrode is passive.

The corona is a non-equilibrium plasma and has a low degree of ionization (about 10^{-8}%). Electrons absorb most of the energy supplied to the plasma. Energy transfer from electrons to heavy species is inefficient due to the differences in their masses. As a result, the electron mean temperature is much higher than the temperature of heavy species. Electrons transfer energy by Coulomb collisions among themselves and dissipate energy by inelastic collisions with heavy species. Due to the low concentration of

electrons, Coulomb collisions are insufficient to maintain a Maxwellian distribution of electrons.

3. MODELING OF THE DC CORONA PLASMA

3.1. Prior Modeling Efforts

Most of the earlier models of the dc corona discharge consider only the unipolar ion region.[32–39] Sarma and Janischewskyj[40] were the first to model the electric field distribution within the thin corona plasma. Their results show that in both positive and negative corona plasma regions, the electric field is not distorted by the space charge for current densities as high as $10\,\mu A/cm$. Evans and Inculet[41] measured the size of the visible ionization layer and found that the ionization region is thicker for negative discharges than that for positive discharges. Landers[29] and Takahashi *et al.*[30] calculated the current and charge carrier distributions for a wire-cylinder. They solved the governing equations for the entire interelectrode space to determine the electron density distribution. However, neither considered the diffusion of electrons, which based on our results increases the number density of electrons close to the discharge electrode. To our knowledge, this paper presents the first numerical model of the electron energy distribution in the dc corona plasma.

3.2. Modeling Approach

The corona plasma extends a short distance (2 to 10 wire radii depending on wire size) beyond the wire surface. Consequently, it is reasonable to model the ionization region as a thin cylindrical annulus, which is one-dimensional in the radial direction. The computational domain, shown in Fig. 2, extends from the wire surface ($r = a$) to the outside radius ($r = r_0$)

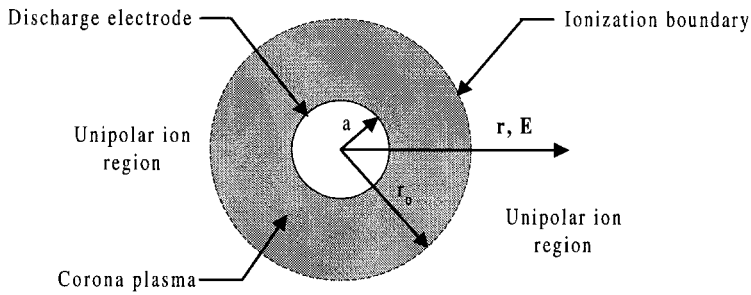

Fig. 2. The computational domain is a thin cylindrical annulus that includes only the corona ionization region. It is bounded by the wire surface at $r = a$ and the outside edge of the corona at $r = r_0$.

of the corona plasma. The ionization boundary, which must be determined, is defined by the radial position where the ionization coefficient and the attachment coefficient, given by Eqs. (5 or 6) and (7), are equal. This equality exists at an electric field strength of $\sim 3 \times 10^6$ V/m. The interelectrode spacing affects only the total current, which is used to specify the boundary condition for charge carrier density distributions.

3.2.1. Electron Density and Electric Field Distributions

In the cylindrical coordinate system, the simplified 1-D governing equations in the steady-state plasma region are conservation of charge for electrons, positive ions and negative ions, given in Eqs. (1)–(3), respectively, and Maxwell's Eq. (4), which relates the electric field to the charge carrier densities.

$$\frac{d(rn_e\mu_e E)}{r\,dr} + \frac{d}{r\,dr}\left(rD_e\frac{dn_e}{dr}\right) = -(\alpha - \beta)n_e\mu_e E \tag{1}$$

$$\frac{d(rn_p\mu_p E)}{r\,dr} = \alpha n_e\mu_e E \tag{2}$$

$$\frac{d(rn_n\mu_n E)}{r\,dr} = -\beta n_e\mu_e E \tag{3}$$

$$\frac{d(rE)}{r\,dr} = \frac{e(n_p - n_e - n_n)}{\varepsilon_0} \tag{4}$$

In these equations, n_e, n_p, and n_n are the number density of electrons, positive ions and negative ions, respectively; μ_e, μ_p, and μ_n are the mobility of electrons, positve ions and negative ions, respectively; E is the local electric field strength; α and β are the ionization coefficient and the attachment coefficient of electrons; D_e is the diffusion coefficient of electrons; and ε_0 is the permittivity of the free space.

The continuity Eqs. (1)–(3) neglect recombination of positive and negative charges and diffusion of ions. The diffusion coefficients of positive and negative ions are two orders of magnitude less than that of electrons.[42] Diffusion of electrons is not negligible, particularly near the wire surface, and is included in Eq. (1). Our results indicate that the electron density is an order of magnitude lower if diffusion of electrons is not considered.

The ionization coefficient (α), attachment coefficient (β), mobility (μ_e), and diffusion coefficient (D_e) of electrons depend on the magnitude of the electric field, pressure and temperature. Empirical correlations for α are expressed in Eqs. (5) and (6) for dry air at atmospheric pressure and

293 K.[43] The value of electric field is in units of V/m.

$$\alpha = 3.63 \times 10^5 \exp(-1.68 \times 10^7/E)\ 1/\text{m} \quad (19.25 \times 10^5 \le E \le 45.6 \times 10^5\ \text{V/m}) \tag{5}$$

$$\alpha = 7.36 \times 10^5 \exp(-2.01 \times 10^7/E)\ 1/\text{m} \quad (45.6 \times 10^5 \le E \le 190.5 \times 10^5\ \text{V/m}) \tag{6}$$

The value of the attachment coefficient is given by

$$\beta = 1.482 \times 10^3 \exp(-3.465 \times 10^6/E)\ 1/\text{m}^{(44)} \tag{7}$$

An expression for electron mobility was obtained from a curve fit of data plotted in[45]

$$\mu_e = 1.2365 E^{-0.2165}\ \text{m}^2/\text{V-s with } R^2 = 0.9942 \tag{8}$$

The diffusion coefficient of electrons is determined from

$$D_e = \int_0^\infty \frac{2eu^{3/2}}{3m_e \nu_m} f_0(u)\, du \tag{9a}$$

where the electron energy distribution function, $f_0(u)$, is determined from solution of the simplified Boltzmann equation presented in Section 3.2.2. The result, expressed as a function of electric field strength, is

$$D_e = 0.0684 \ln(E) - 0.8678\ \text{m}^2/\text{s} \tag{9b}$$

Ion mobility is assumed to be constant.[42,45,46] For positive and negative ions, the mobility is 2.0×10^{-4} and $2.7 \times 10^{-4}\ \text{m}^2/\text{V-s}$, respectively.

Because the diffusion of electrons is included in this analysis, Eq. (1) requires two boundary conditions. The first boundary condition is at the wire surface. The electron distribution at $r = a$ is expressed in terms of the current density per unit surface (J), which is the sum of the electron drift current and the diffusion current.

$$J(a) = e\left[\mu_e(a) E(a) n_e(a) + D_e(a) \left.\frac{dn_e}{dr}\right|_{r=a}\right]. \tag{10}$$

The total current density $J(a)$ is easily measured at the grounded electrode. The electric field strength $E(a)$ is assumed equal to the value given by Peek's empirical dimensional formula for the onset field.

$$E(a) = E_i = 3 \times 10^6 \varepsilon\left(\delta + 0.03\sqrt{\frac{\delta}{a}}\right)\text{V/m} \tag{11}$$

where the wire radius a is expressed in meters, ε is the dimensionless surface roughness of the electrode ($\varepsilon = 1$ for smooth surfaces), and δ is the relative

density of air ($\delta = T_0 P / T P_0$), where T_0 and P_0 are reference temperature (293 K) and pressure (101,325 Pa) respectively. The assumption that the electric field strength at the wire equals Peek's onset field is generally accepted and justified by Morrow.[47]

The second boundary condition is specified at the outside edge of the plasma. The number density of electrons at the outside edge of the corona plasma is assumed equal to the electrons produced by photoionization,[40]

$$n_e(r_0) = \gamma_p \int_a^{r_0} \alpha(r) g(r)\, e^{-\mu(r_0 - r)} n_e(r)\, dr \tag{12a}$$

where the geometric factor, $g(r)$, represents the fraction of photons produced at position r that reaches the outer edge of the corona at $r = r_0$. This factor is the product of the radial and axial geometric factors.[48]

$$g(r) = g_{\text{radial}}(r) \cdot g_{\text{axial}}(r) \tag{12b}$$

where

$$g_{\text{radial}}(r) = \frac{1}{\pi\, e^{-\mu(r_0 - r)}} \int_0^{\pi - \sin^{-1}(a/r)} e^{-\mu(r_0^2 + r^2 - 2 r_0 r \cos\phi)^{1/2}}\, d\phi \tag{12c}$$

and

$$g_{\text{axial}}(r) = \frac{2}{\pi\, e^{-\mu(r_0 - r)}} \int_0^{\pi/2} e^{-\mu(r_0 - r)/\cos\phi}\, d\phi \tag{12d}$$

γ_p is the photoionization coefficient, and μ is the absorption coefficient for photons in air (6 cm^{-1}).

Only one boundary condition is required for conservation of ions given by Eqs. (2) and (3). Since positive ions do not contribute to the total current at the wire surface, their density is zero there and the boundary condition for Eq. (2) is

$$n_p(a) = 0 \tag{13}$$

The boundary condition for Eq. (3) is the number density of negative ions at the outside edge of the corona. The numerical value is unknown; however it is reasonable to assume the number density of negative ions is less than the number density of electrons at one atmosphere (1×10^9 m^{-3}). The results discussed in this paper were determined for a negative ion density at the outside boundary of the plasma equal to

$$n_n(r_0) = 1 \times 10^8\ \text{m}^{-3} \tag{14}$$

We found that the calculated electron density and electric field distributions did not change for $1\,\mathrm{m}^{-3} < n_n(r_0) < 1 \times 10^9\,\mathrm{m}^{-3}$.

Maxwell's Eq. (4) requires one boundary condition at the wire surface. Specification of an additional boundary condition at the outer edge of the corona permits us to determine the position of this boundary by iteration. The electric field at the outside radius of the plasma (r_0) is determined by equating the ionization coefficient to the attachment coefficient. This model uses the value agreed upon by most researchers,[49,50]

$$E(r_0) = 3 \times 10^6\,\mathrm{V/m} \tag{15}$$

Equations (1)–(4) are solved using the central finite-difference method programmed in FORTRAN. Non-uniform grids are generated along the radial direction. A very fine grid is required close to the discharge wire surface to accurately model the extremely high electron density gradient there. The final grid size is sufficiently fine so that further refinement did not produce changes in the computed electron density and electric field. The total number of grids used is 10,000, with a $10^{-5}\,\mu$m grid next to the wire surface and a $0.01\,\mu$m grid at the outside edge of the corona.

For a given wire radius and linear current density (expressed as total current per unit length of wire, $I = 2\pi a \cdot J\,\mathrm{A/m}$), an initial electric field distribution is assumed. For fast convergence, the initial electric field s assigned as the electrostatic field in the absence of space charge ($E(r) = aE_i/r$). Once the electric field is determined, the ionization coefficient Eqn. (5 or 6), attachment coefficient (7), mobility (8) and the diffusion coefficient (9) of electrons are determined. The electron density, positive ion density and the negative ion density are then calculated at various radii in the plasma region according to Eqs. (1)–(3). A new electric field distribution is obtained using the Maxwell's Eq. (4). If the new electric field distribution is different from the old electric field distribution, iteration is performed. This iteration terminates when the difference between the old electric field and the new electric field is less than $10^{-3}\%$ of the old value for every radial position.

The plasma thickness is also calculated by iteration. An initial plasma thickness is assumed, and then a convergent solution for the electric field is obtained using the known electric field at the electrode surface as the boundary condition. The iterations are terminated when the calculated electric field at the outside edge of the plasma is within 0.01% of $3 \times 10^6\,\mathrm{V/m}$. Finally, the plasma thickness, the distributions of electric field, electron density, positive ion density and negative ion density are uniquely determined for a given wire radius and current.

3.2.2. Electron Energy Distribution

The electron energy distribution is governed by the Boltzmann equation,[51]

$$\frac{\partial F}{\partial t} + \mathbf{v} \cdot \nabla_r F + \mathbf{a} \cdot \nabla_v F = \left(\frac{dF}{dt}\right)_c \tag{16}$$

where F is the electron distribution function, $\mathbf{v}$ is the electron velocity, and $\mathbf{a}$ is the acceleration of electrons ($\mathbf{a} = -e\mathbf{E}/m_e$). For a strongly collisional plasma, like the corona, Kortshagen[52] shows that a local approximation $(\partial/\partial r)(\,) = 0$ is valid because the effect of spatial inhomogeneity is relatively unimportant compared with the collisional effect. In the corona plasma, elastic collisions are more frequent than inelastic collisions. Electrons lose little energy during elastic collisions because their mass is much smaller than that of heavy species present. Consequently, the direction of the electron velocity changes but the speed remains nearly constant after elastic collisions. In addition, the electron drift velocity is relatively small compared to the electron mean thermal speed, and the electron distribution is nearly isotropic in velocity space. Thus, the two-term Legendre expansion for the electron velocity distribution is valid.[51] At each radial position, the electron energy distribution in the corona plasma can be obtained by solving the spatially homogeneous Boltzmann equation,

$$\frac{2e}{3m_e}\frac{\partial}{\partial u}\left[\frac{u^{3/2}E^2}{\nu_m}\frac{\partial f_0}{\partial u} + \frac{3m_e^2 u^{3/2}\nu_m f_0}{eM_h}\right] + u^{1/2}Q(f_0) = 0 \tag{17}$$

where f_0 is the electron energy distribution function (EEDF), m_e and M_h are the mass of electrons and heavy species respectively, u is the electron kinetic energy, ν_m is the elastic collision frequency of electrons, and $Q(f_0)$ is the inelastic collision integral. This expression shows that the EEDF depends only on the electric field for the corona plasma in air. The boundary conditions for Eq. (17) can be specified at the zero kinetic energy and the infinitely large kinetic energy,

$$f_0(0) = 0 \quad \text{and} \quad f_0(\infty) = 0 \tag{18}$$

In this study, the upper bound of the kinetic energy is assumed to be 150 eV, which is over ten times the maximum mean kinetic energy of electrons in the corona plasma and considered equal to infinity.

The collision integral $Q(f_0)$ includes the inelastic collisions in the corona discharge that dominate changes in the electron energy distribution. In Eqs. (19)–(22), $Q_{ex}^{k}(f_0)$, $Q_{dis}(f_0)$, $Q_{att}(f_0)$, and $Q_i(f_0)$ are collision

integrals for the kth excitation, dissociation, attachment, and ionization, respectively.

$$Q_{\mathrm{ex}}^{k}(f_0) = \sum_{k}\left(-f_0(u)\nu_{\mathrm{ex}}^{k}(u) + \sqrt{\frac{u+u_k}{u}}\, f_0(u+u_k)\nu_{\mathrm{ex}}^{k}(u+u_k)\right) \tag{19}$$

$$Q_{\mathrm{dis}}(f_0) = -f_0(u)\nu_{\mathrm{dis}}(u) + \sqrt{\frac{u+u_{\mathrm{dis}}}{u}}\, f_0(u+u_{\mathrm{dis}})\nu_{\mathrm{dis}}(u+u_{\mathrm{dis}}) \tag{20}$$

$$Q_{\mathrm{att}}(f_0) = -f_0(u)\nu_{\mathrm{att}}(u) \tag{21}$$

$$Q_{\mathrm{i}}(f_0) = -f_0(u)\nu_{\mathrm{i}}(u) + 4\sqrt{\frac{2u+u_{\mathrm{i}}}{u}}\, f_0(2u+u_{\mathrm{i}})\nu_{\mathrm{i}}(2u+u_{\mathrm{i}}) \tag{22}$$

In these expressions, u_k and u_{dis} are the energy threshold for the kth excitation and dissociation, respectively; u_{i} is the ionization potential; ν_{ex}, ν_{dis}, ν_{att}, and ν_{i} are the collision frequency for excitation, dissociation, attachment, and ionization, respectively. The collision frequency is defined as,

$$\nu(u) = \sqrt{\frac{2e}{m_{\mathrm{e}}}}\, n_{\mathrm{h}} u^{1/2}\sigma(u) \tag{23}$$

where n_{h} is the density of the heavy species and $\sigma(u)$ is the collision cross-section for electrons with a kinetic energy u. Each collision integral for inelastic collisions takes into account the loss of electrons with kinetic energy u and the gain of electrons scattered into this energy level from other energy levels due to inelastic collisions. For ionizations, new electrons produced are assumed to have the same kinetic energy as primary electrons after the collision.

The original finite-difference source code for the numerical solution of the time-dependent homogeneous Boltzmann equation was developed by Kortshagen[53] in the "C" programming language. It was rewritten for this work in FORTRAN. The input data are electric field, neutral densities, molecular weight of heavy species, and electron collision cross-sections in air. The neutral (O_2 and N_2) densities used in these calculations are those for atmospheric pressure, with 21% O_2 and 79% N_2. The spatial distribution of the electric field is calculated as described in Section 3.2.1. Electron collision cross-sections are those compiled by Phelps and his coworkers at the Joint Institute for Laboratory Astrophysics (JILA), Colorado.[54–56]

The grid size generated in the kinetic energy space is 0.05 eV, with 3000 meshes from 0 to 150 eV. A Maxwellian distribution of electrons with a mean kinetic energy of 11 eV is used as a first guess. Iteration is terminated

when the new distribution function at any energy differs from the old distribution function by less than $10^{-6}\%$. Once a convergent distribution function is obtained, it is normalized so that $\int_0^\infty u^{1/2} f_0(u)\, du = 1$.

4. RESULTS AND DISCUSSION

Electric field, charge carrier number density and electron energy distributions in the positive corona plasma were obtained for six wire radii (10, 50, 100, 200, 500, and 1000 μm) and six linear current densities (0.1, 1, 2.55, 5, 10, and 100 μA/cm). These values provide a sufficient range to represent the most common uses of dc coronas. It is unlikely that the current would ever exceed 100 μA/cm without sparkover. Distributions of electron number density, ion number density, current density, electric field and electron energy in the corona plasma are presented for a dc positive discharge from a 100 μm-radius wire, with a current density of 2.55 μA/cm in Sections 4.1 to 4.3. This wire size and current density are typical for indoor electrostatic precipitators. The shapes of distributions computed for the other cases considered are similar. Empirical correlations for electric field, plasma thickness and electron mean kinetic energy for corona plasmas are provided.

Both the wire radius and the current density influence the electron distribution in the corona plasma and thus the rate of chemical reactions involving electrons. The wire radius determines the electric field at the discharge wire surface according to Peek's equation, and the current density defines the electron density at the plasma boundary. The effect of changes in current density on the distribution of electrons is presented in Section 4.4. The effect of wire diameter is presented in Section 4.5. The effect of electrode size on the electron-impact chemical reaction rate is illustrated with the rates of dissociation and ionization of oxygen and nitrogen.

4.1. Charge Carrier Number Density and Current Density Distributions

The distributions of the electron and ion number densities with respect to the distance from the wire surface are plotted in Fig. 3 for a 100 μm-radius wire with a linear current density of 2.55 μA/cm of wire. The corona initiation electric field E_i is 1.2×10^7 V/m and the plasma is three wire radii or 300 μm thick.

Electron and negative ion densities decrease sharply very near the wire surface. The electron density drops four orders of magnitude from $5.4 \times 10^{13}\,\mathrm{m}^{-3}$ at the wire surface to $5.5 \times 10^{9}\,\mathrm{m}^{-3}$ 60 μm away. The density of negative ions drops two orders of magnitude from $6.6 \times 10^{12}\,\mathrm{m}^{-3}$ to $2.2 \times 10^{10}\,\mathrm{m}^{-3}$ in the same distance. The positive ion density rises very rapidly from zero at the wire surface to $1.0 \times 10^{15}\,\mathrm{m}^{-3}$ only 5 μm away.

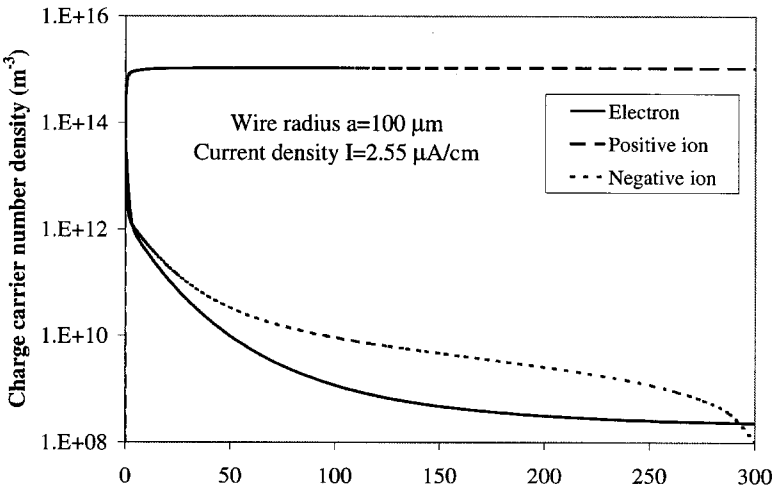

Fig. 3. Charge carrier number density distribution in the corona plasma plotted for a 100 μm radius wire with a current per unit length of wire equal to 2.55 μA/cm.

Throughout the remainder of the 300 μm thick corona, the density of positive ions remains nearly constant and at least five orders of magnitude higher than the densities of negative ions and electrons. These trends are qualitatively similar to the results obtained by Takahashi *et al.*[30] However, our results show that electron diffusion increases the electron density near the wire surface one order of magnitude. Figure 4 shows that the diffusion of electrons produces a negative current within four microns of the wire surface. Thus, the electron drift current ($e\mu_e En_e$) must increase to keep the total current constant according to Eq. (10), and the electron density near the wire surface increases.

The current density distribution due to positive and negative ions as well as electrons is plotted in Fig. 5. The positive ion current density increases rapidly close to the wire and the total current is carried by positive ions at about 25 μm. Because of their low mobility, negative ions do not contribute to the current, even close to the wire where the density of negative ions is relatively high. In agreement with Landers' results,[29] electrons are responsible for the total current at the wire surface, but carry only 6% of the total current 10 μm away from the wire surface.

4.2. Electric Field Distribution

The electric field distribution is plotted in Fig. 6 for zero current and linear current densities of 0.1, 1, 2.55, 5, 10, and 100 μA/cm. The distribution for current densities $\leq 10\,\mu$A/cm are nearly identical to the

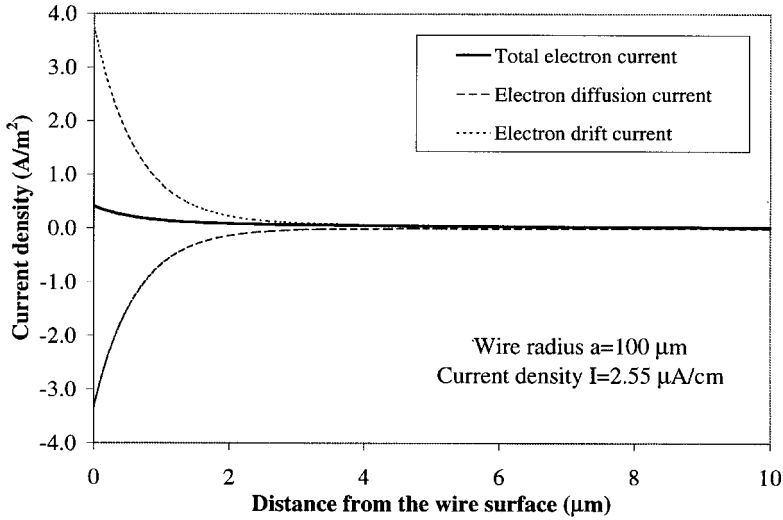

Fig. 4. Composition of the electron current shown as the electron drift current ($e\mu_e En_e$) and the electron diffusion current ($eD_e dn_e/dr$). This plot is for a 100 μm radius wire with a current per unit length of wire equal to 2.55 μA/cm.

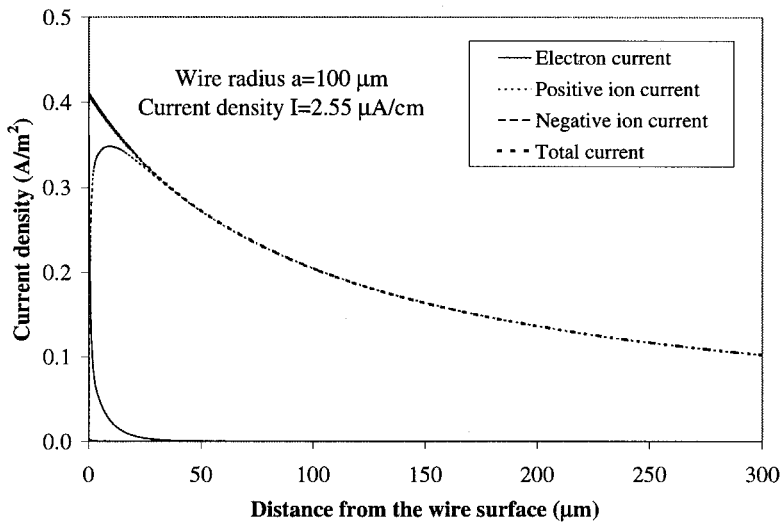

Fig. 5. Total current density distribution and current density distributions due to electrons and ions. This plot is for a 100 μm radius wire with a current per unit length of wire equal to 2.55 μA/cm. The negative ion current density is so small that is practically invisible on this plot.

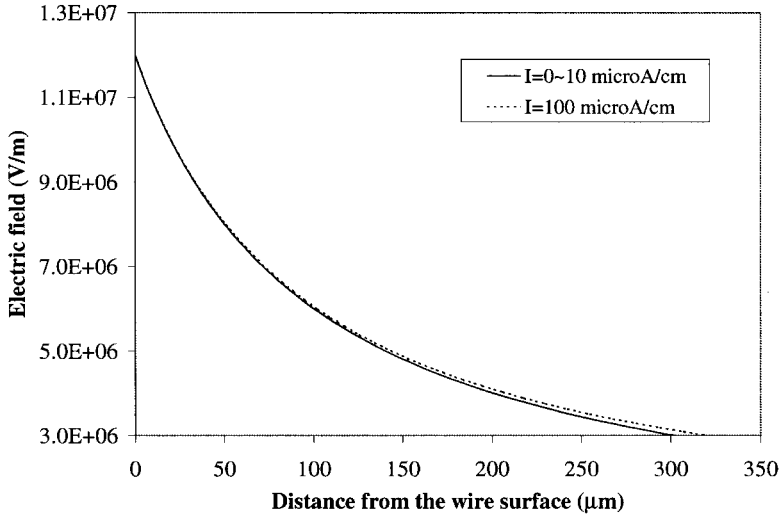

Fig. 6. Electric field distribution for a 100 μm radius wire. Data are for current densities of 0, 0.1, 1, 2.55, 5, 10, and 100 μA/cm.

distribution with no space charge. There is a small variation ($< 5\%$) at 100 μA/cm. This result is consistent with that of Sarma and Janischewskyj[40] and is explained by the relatively low space charge density throughout the plasma region. Thus, for typical applications of dc coronas, the electric field in the corona plasma can be approximated as,

$$E(r) = \frac{E_i a}{r} \tag{24}$$

where r is the radial position. Since the outside edge of the corona plasma is defined by the electric field $E_0 = 3 \times 10^6$ V/m at which the ionization balances the attachment, the outer radius of the plasma (r_0) can be expressed as,

$$r_0 = \frac{E_i a}{E_0} \tag{25}$$

4.3. Electron Energy Distribution

The one-dimensional electron kinetic energy distribution (from 0 to 50 eV) is plotted in Fig. 7. With increasing distance from the discharge wire, the mean kinetic energy of electrons decreases due to the rapidly decreasing electric field. At the outside edge of the plasma, the mean kinetic energy of electrons is 3.19 eV, which is about 34% of the mean kinetic energy for electrons near the wire surface (9.37 eV).

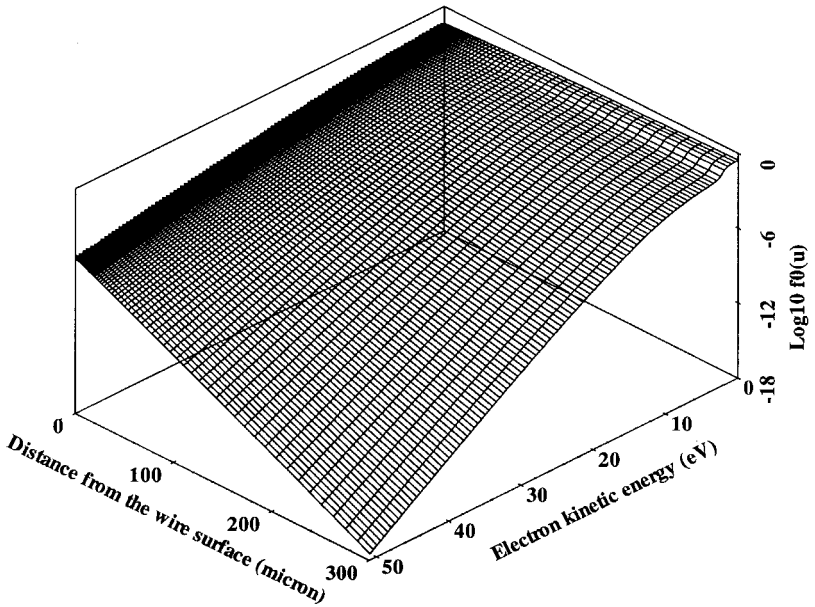

Fig. 7. Electron kinetic energy distribution across the corona plasma for wire radius $a = 100\ \mu$m and current density $I = 2.55\ \mu$A/cm.

The computed electron energy distributions at both boundaries of the corona plasma ($r = a$ and $r = r_0$) are compared to values predicted by a Maxwellian distribution in Fig. 8. The deviation from a Maxwellian distribution with the same mean kinetic energy increases with increasing electron kinetic energy. The population of electrons at high energies is lower than that for the corresponding Maxwellian distribution because elastic collisions between electrons are insufficient to recover the lost energy of electrons that have undergone inelastic collisions. The energy distribution of electrons at the outside edge of the corona plasma is steeper than that of electrons near the discharge surface. Electrons at the outer edge of the plasma have a lower mean kinetic energy than do those very close to the discharge surface.

For electron-impact reactions with significant collision cross-sections at high energies, such as electron-impact ionizations, the reaction rate would be overestimated if a Maxwellian distribution is assumed. However, because only about 5% of the electrons are in the high-energy region that deviates from a Maxwellian distribution, in some situations, for example, when the electron-impact collision cross-sections are negligible at high energies (e.g., rotational excitations), it is useful to approximate the electron kinetic energy distribution as Maxwellian. In this circumstance, the mean kinetic energy

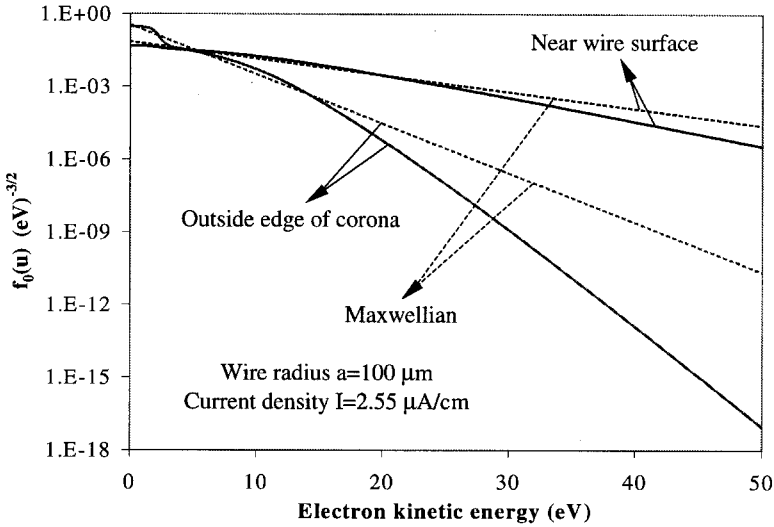

Fig. 8. The calculated distribution of the electron kinetic energy in the immediate vicinity of the wire and at the outside edge of the corona compared to a Maxwellian distribution.

may be used to characterize the energy distribution of electrons and an empirical correlation for the electron mean kinetic energy is of practical use. The mean kinetic energy of electrons depends only on the electric field and is curve fit in Fig. 9.

4.4. Effect of Current Density on Electron Distribution

The effect of current density is studied for a 100 μm radius wire. The number density of electrons is plotted as a function of distance from the wire surface for linear current densities of 0.1, 1, 2.55, 5, 10, and 100 μA/cm in Fig. 10. The plot shows two important results. The size of the corona plasma is independent of current for practical current densities below 10 μA/cm, and the electron density increases with the increasing current density throughout the plasma. Takahashi *et al.*[30] point out that there is no agreement in the literature on the effect of current on the thickness of the corona. However, our numerical results, which indicate there is no effect, agree with their results. In addition, the thickness of the corona has little impact on total chemical reaction rates because the highest density and most energetic electrons are near the surface of the discharge electrode.

As shown in Fig. 11, changes in current density have no influence on the mean kinetic energy distribution of electrons for current densities as

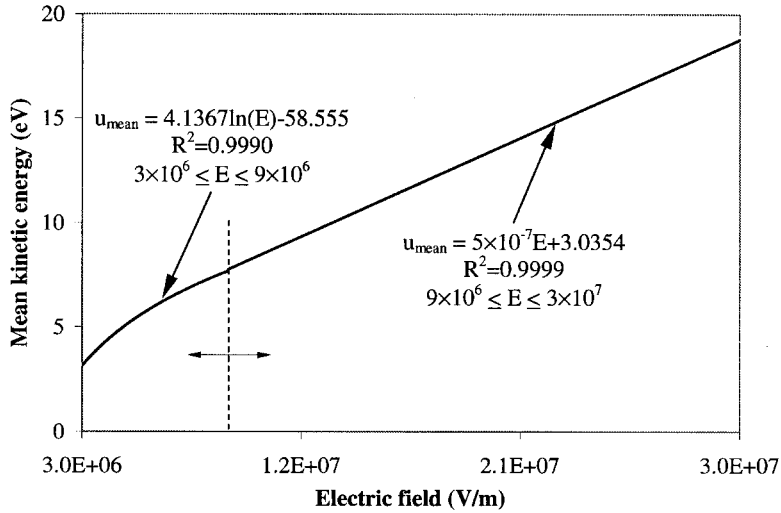

Fig. 9. The electron mean kinetic energy as a function of electric field for a Maxwellian distribution with the same mean kinetic energy as the calculated distribution.

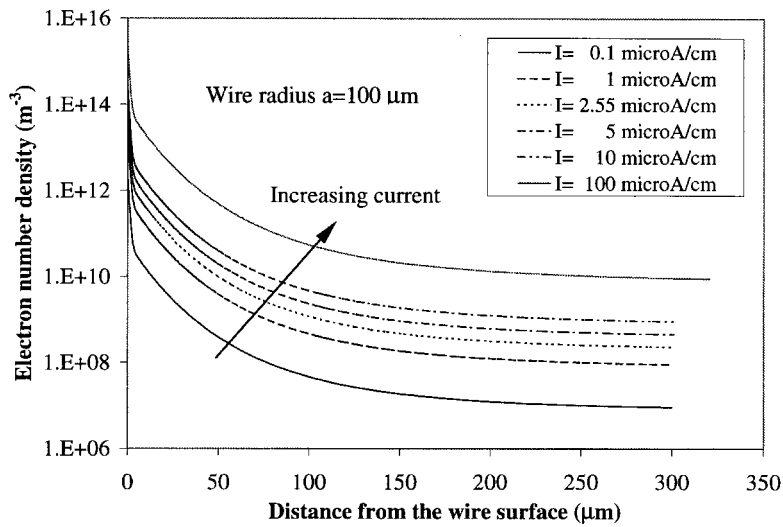

Fig. 10. Effect of the current density on the electron density distribution for a wire radius equal to 100 μm.

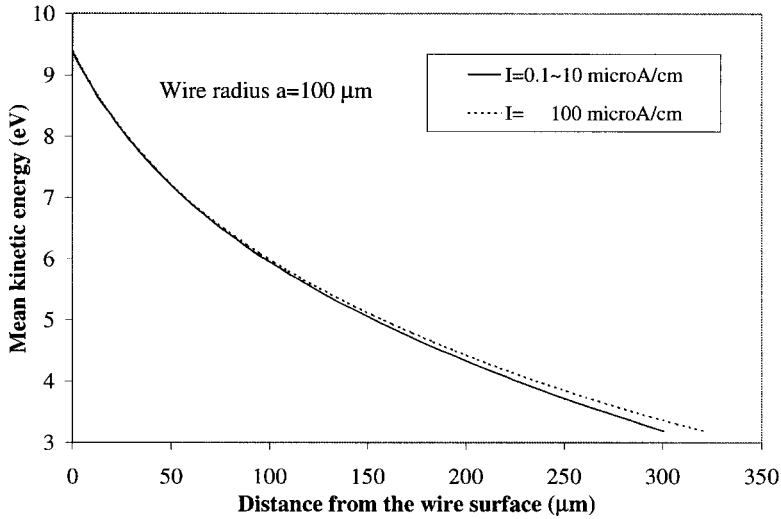

Fig. 11. Effect of the current level on the mean kinetic energy distribution of electrons. Data are plotted for linear current densities of 0.1, 1, 2.55, 5, 10, and 100 μA/cm.

high as 10 μA/cm. From 10 μA/cm to 100 μA/cm, the mean kinetic energy increases a maximum of 5% 300 μm away from the wire surface. However, the total number of electrons produced increases and the rate of electron-impact chemical reactions increases with increasing current level.

4.5. Effect of Wire Radius on Electron Distribution

The effect of wire radius on electron density distributions is shown in Fig. 12. These data were computed with a fixed current density at the wire surface (0.406 A/m^2, equivalent to a linear current density of 2.55 μA/cm for a 100 μm-radius wire) for wire radii equal to 10, 50, 100, 200, 500, and 1000 μm. Both electron density and plasma thickness increase with increasing wire size. The rate of decrease of electron density with distance increases with decreasing wire size because the gradient in electric field increases. The total number of electrons increases with increasing wire size. The plasma thickness is plotted in Fig. 13 as a function of wire radius. This relationship between the thickness of the corona and the wire size agrees qualitatively with Evans and Inculet[41] and Takahashi *et al.*[30]

Figure 14 is a plot of the mean kinetic energy of electrons as a function of radial distance from the wire surface for the six wire radii considered. The mean kinetic energy of electrons near the wire surface is higher for

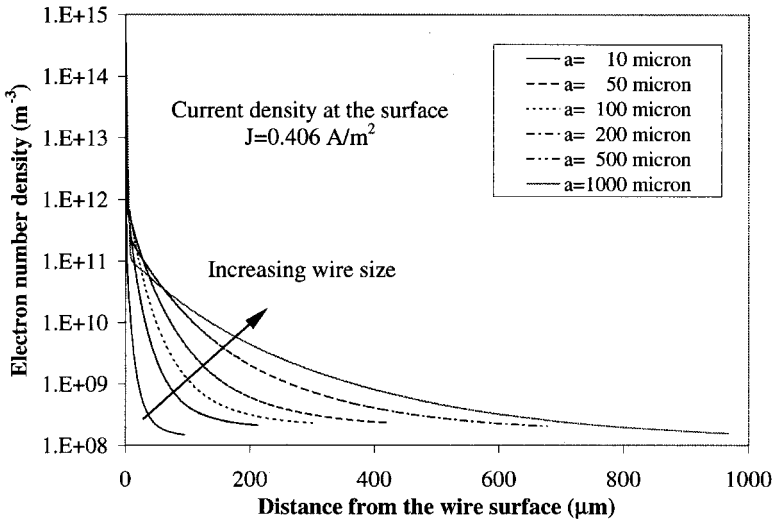

Fig. 12. Effect of the wire size on the electron density distribution for a wire surface current density of 0.406 A/m^2.

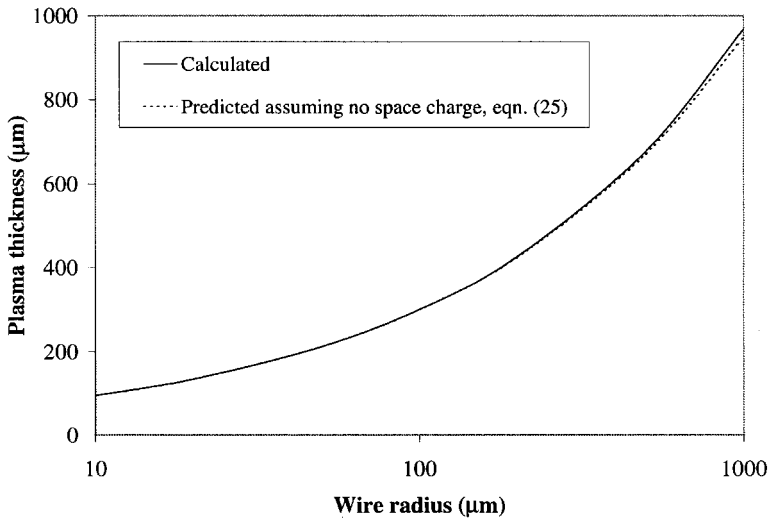

Fig. 13. The effect of the wire size on the thickness of the corona plasma for a wire surface current density of 0.406 A/m^2.

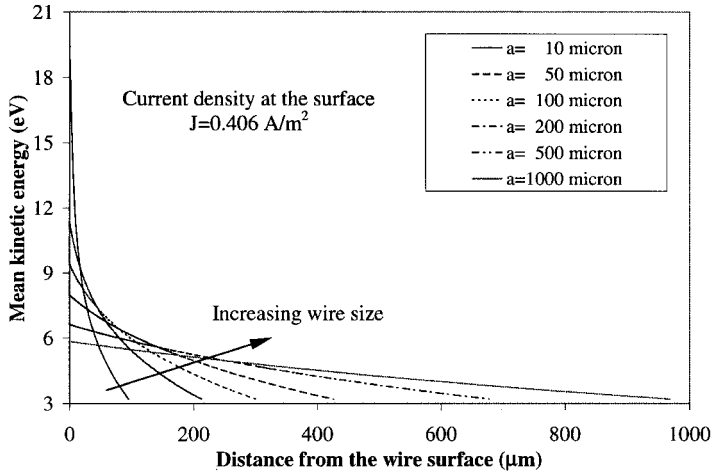

Fig. 14. Effect of the wire size on the electron mean kinetic energy distribution for a wire surface current density of 0.406 A/m^2.

smaller wires, but decreases rapidly with distance because the corona plasma is thinner. Electrons at the outside edge of the corona plasma have the same mean kinetic energy (3.19 eV) for all wire sizes because of the same electric field there. Since the chemical reaction rate depends on both electron density and electron energy, whether small wires or larger wires are more favorable for chemical reactions depends on the reaction.

To elucidate the effect of the wire size on the electron-impact reaction rate, the reaction rates for dissociation and ionization of O_2 and N_2 molecules are analyzed for the same six wire radii. The local reaction rate and the total reaction rate per unit length of wire are expressed in Eqs. (26) and (27), respectively,

$$\Re(r) = n_e(r) n_h(r) \int_{u_{th}}^{\infty} \sqrt{\frac{2eu}{m_e}}\, \sigma(u) f_0(u) u^{1/2}\, du \tag{26}$$

$$\frac{\Re_{tot}}{L} = \int_a^{r_0} \Re_{loc}(r) \cdot 2\pi r\, dr \tag{27}$$

where $\Re(r)$ is the local reaction rate at radial position r and $\Re_{tot}$ is the total reaction rate in the whole ionization region; u_{th} is the energy threshold for the reaction (u_{th} equals 5.6, 9.8, 12.06, and 15.6 eV for dissociation of O_2, dissociation of N_2, ionization of O_2, and ionization of N_2, respectively); and L is the length of the wire. These reaction rates are not actual reaction rates since reverse reactions are not considered. The calculated results are

plotted in Fig. 15. When the energy threshold for the reaction is low, for instance, for the dissociation of O_2, the reaction rate increases monotonically with increasing wire size. This result is consistent with the experimental data for production of ozone from positive coronas.[11] However, this trend is not true for the dissociation of N_2 and ionization of O_2 and N_2, which are reactions with higher energy thresholds. For these reactions, there is an optimum wire size that maximizes the reaction rate.

5. CONCLUSION

The corona discharge produces a thin plasma, which is bounded by the high-voltage discharge electrode surface and an imaginary outside boundary where the ionization process balances the electron attachment process. The electron distribution in the corona plasma exhibits a strong spatial nonuniformity, especially in the vicinity of the discharge electrode. For a positive wire discharge, the electron density is highest near the wire and decreases rapidly with increasing distance from the surface. The diffusion of electrons is significant near the high-voltage electrode and cannot be neglected in terms of electron number density distribution.

Although the corona plasma has a net space charge, the distortion of the electric field due to the space charge is negligible for current densities up to 10 μA/cm. For most applications, the electric field distribution in the corona plasma is Laplacian ($r \cdot E(r) = \text{const.}$) and the thickness of the

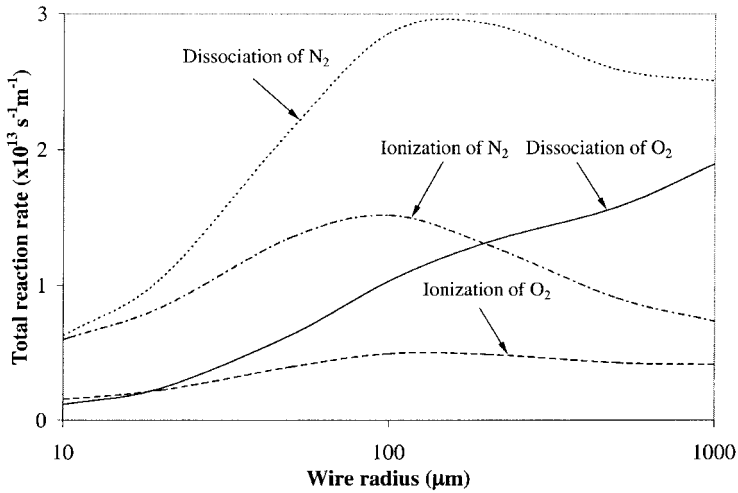

Fig. 15. Effect of wire size on the total reaction rate per unit wire length for dissociation and ionization of O_2 and N_2 molecules.

plasma is predicted as $r_0 = E_i a/E_0$ with $E_0 = 3 \times 10^6$ V/m. The electron energy distribution is non-Maxwellian, with a lower population at the high-energy tail. The electron kinetic energy distribution is uniquely determined by the local electric field for atmospheric air corona. The electron mean kinetic energy is on the order of several eV and it increases with increasing electric field strength. The most energetic electrons are produced near the high-voltage electrode. Those energetic electrons can easily induce chemical reactions.

Both the current level and wire size affect the electron distribution in the corona plasma. For a given wire size, higher current levels produce more electrons but the plasma thickness and electron energy distribution remain unchanged for increasing current levels up to 10 μA/cm. This result implies that the electron-impact chemical reaction rate increases with the increasing current levels for a given wire radius.

Smaller electrodes produce thinner plasmas and fewer electrons, but the electrons have a higher mean kinetic energy than those produced with larger wires. Thus, the effect of electrode size on the electron-impact chemical reaction rate depends on the energy threshold of the reaction.

NOMENCLATURE

σ	collision cross-section, m^2
β	electron attachment coefficient, m^{-1}
α	first Townsend ionization coefficient, m^{-1}
δ	relative density of air, $T_0 P/TP_0$
ν	collision frequency, s^{-1}
ε	surface roughness, $\varepsilon = 1$ for smooth surfaces
ν_{att}	collision frequency for attachments, s^{-1}
ν_{dis}	collision frequency for dissocations, s^{-1}
μ_e	electron mobility, $m^2\,V^{-1}\,s^{-1}$
ν_{ex}^k	collision frequency for kth excitations, s^{-1}
ν_i	collision frequency for ionizations, s^{-1}
ν_m	elastic collision frequency, s^{-1}
μ_n	negative ion mobility, $m^2\,V^{-1}\,s^{-1}$
ε_0	permittivity of the free space, 8.86×10^{-12} F/m
μ_p	positive ion mobility, $m^2\,V^{-1}\,s^{-1}$
γ_p	photoionization coefficient
a	acceleration vector, m/s^2
a	wire radius, m
μ	absorption coefficient for photons in air, $6\,cm^{-1}$
D_e	diffusion coefficient of electrons, $m^2\,s^{-1}$

e	elementary charge, 1.6×10^{-19} C
$\mathbf{E}$	electric field vector, V/m
E	electric field, V/m
E_i	electric field at the electrode surface, V/m
E_0	electric field at the outside edge of the corona, V/m
F	electron distribution function
$f_0(u)$	electron energy distribution function, $\mathrm{eV}^{-3/2}$
g	total geometrical factor
g_{axial}	axial geometrical factor
g_{radial}	radial geometrical factor
I	linear current density, A/m
J	area current density, $\mathrm{A/m^2}$
L	length of the wire, m
m_{e}	electron mass, 9.1×10^{-31} kg
M_{h}	mass of the heavy species molecule, kg
n_{e}	electron number density, $\mathrm{m^{-3}}$
n_{h}	number density of heavy species, $\mathrm{m^{-3}}$
n_{n}	negative ion number density, $\mathrm{m^{-3}}$
n_{p}	positive ion number density, $\mathrm{m^{-3}}$
P	pressure, Pa
P_0	reference pressure, 101,325 Pa
Q	inelastic collision integral, $\mathrm{eV^{-3/2}\,s^{-1}}$
Q_{att}	collision integrals for attachments, $\mathrm{eV^{-3/2}\,s^{-1}}$
Q_{dis}	collision integrals for dissociations, $\mathrm{eV^{-3/2}\,s^{-1}}$
Q_{ex}^{k}	collision integrals for kth excitations, $\mathrm{eV^{-3/2}\,s^{-1}}$
Q_{i}	collision integrals for ionizations, $\mathrm{eV^{-3/2}\,s^{-1}}$
R	correlation coefficient for Eq. (8)
$\Re$	local reaction rate, $\mathrm{m^{-3}\,s^{-1}}$
$\mathbf{r}$	radial position vector, m
r	radial position, m
r_0	radius of the outside edge of the corona, m
$\Re_{\mathrm{tot}}$	total reaction rate, $\mathrm{s^{-1}}$
T	temperature, K
T_0	reference temperature, 293 K
u	electron kinetic energy, eV
u_{dis}	energy threshold for dissociations, eV
u_{i}	ionization potential, eV
u_k	energy threshold for the kth excitation, eV
u_{mean}	electron mean kinetic energy, eV
u_{th}	energy threshold for the reaction, eV
$\mathbf{v}$	electron velocity vector, m/s

ACKNOWLEDGMENT

We gratefully acknowledge the helpful comments and assistance of Dr. Uwe Kortshagen, whose numerical scheme was used to compute the electron energy, and anonymous reviewers whose comments and suggestions were incorported into the final manuscript. The Supercomputing Institute at the University of Minnesota gave financial support in the form of computational time.

REFERENCES

1. B. M. Penetrante, J. N. Bardsley, and M. C. Hsiao, "Kinetic analysis of non-thermal plasmas used for pollution control," *Jpn. J. Appl. Phys.* **36**(Part 1), (7B), 5007–5017 (1997).
2. T. Hammer, "Application of plasma technology in environmental techniques," *Contributions to Plasma Physics* **39**, 441–462 (1999).
3. T. Hammer, "Non-thermal plasma treatment of automotive exhaust gases," in H. Wagner, J. F. Behnke, and G. Babucke (eds.), Proceedings of the International Symposium on High Pressure Low Temperature Plasma Chemistry, Greifswald, Germany, Vol. 2, pp. 234–241, 2000.
4. W. Manheimer, L. E. Sugiyama, and T. H. Stix, *Plasma Science and the Environment*, American Institute of Physics Press, Woodbury, New York (1997).
5. M. L. Balmer, G. Fisher, and J. Hoard, *Non-Thermal Plasma for Exhaust Emission Control: NO_x, HC, and Particulates*, Society of Automotive Engineers, Inc., Warrendale, PA (1999).
6. J. J. Lowke and R. Morrow, "Theoretical analysis of removal of oxides of sulfur and nitrogen in pulsed operation of electrostatic precipators," *IEEE Transactions on Plasma Science* **23**, 661–671 (1995).
7. B. M. Penetrante and S. E. Schultheis, *Non-Thermal Plasma Techniques for Pollution Control Part A: Overview, Fundamentals and Supporting Technologies*, Springer-Verlag, Berlin (1993).
8. B. M. Penetrante and S. E. Schultheis, *Non-Thermal Plasma Techniques for Pollution Control Part B: Electron Beam and Electrical Discharge Processing*, Springer-Verlag, Berlin (1993).
9. A. P. Napartovich, "Critical review of atmospheric pressure discharges producing non-thermal plasma," in H. Wagner, J. F. Behnke, and G. Babucke (eds.), Proceedings of the International Symposium on High Pressure Low Temperature Plasma Chemistry, Greifswald, Germany, Vol. 1, pp. 122–128, 2000.
10. Y. Akishev, S. Kroepke, J. Behnisch, A. Hollander, A. Napartovich, and N. Trushkin, "Non-thermal plasma treatment of polymer films and fabrics based on a glow discharge at atmospheric pressure," in H. Wagner, J. F. Behnke, and G. Babucke (eds.), Proceedings of the International Symposium on High Pressure Low Temperature Plasma Chemistry, Greifswald, Germany, Vol. 2, pp. 481–485, 2000.
11. K. Boelter and J. H. Davidson, "Ozone generation by indoor electrostatic air cleaners," *Aerosol Science and Technology* **27**, 689–708 (1997).
12. J. A. Dorsey and J. H. Davidson, "Ozone production in electrostatic air cleaners with contaminated electrodes," *IEEE Trans. Indus. Applic.* **30**, 370–376 (1994).
13. A. Yehia, A. Mizuno, and K. Takashima, "On the characteristics of the corona discharge in a wire-duct reactor," *J. Phys. D: Appl. Phys.* **33**, 2807–2814 (2000).

14. A. Yehia, M. Abdel-Salam, and A. Mizuno, "On assessment of ozone generation in dc coronas," *J. Phys. D: Appl. Phys.* **33**, 831–835 (2000).
15. R. J. Allen, R. A. Wadden, and E. D. Ross, "Characterization of potential indoor sources of ozone," *Am. Ind. Hyg. Assoc. J.* **39**, 466–471 (1978).
16. K. Nashimoto, "The effect of electrode materials on O_3 and NO_x emissions by corona discharging," *J. Imaging Sci.* **32**, 205–210 (1988).
17. J. Chen and J. H. Davidson, "Effect of silicone concentration on deposition of silicon dioxide in the corona discharge of electrostatic air cleaners," in A. G. Holcomb and P. F. Gebes (eds.), Proceedings of the AFS Air Filtration Fall Conference, (Minneapolis, MN, pp. 203–210, 1999.
18. J. H. Davidson and P. J. McKinney, "Chemical vapor deposition in the corona discharge of electrostatic air cleaners," *Aerosol Science and Technology* **29**, 102–110 (1998).
19. K. Nashimoto, "Growth of SiO_2 needles induced by positive corona discharging," *Jpn. J. Appl. Phys.* **26**, L1138–L1140 (1987).
20. K. Nashimoto, "Growth behavior of silicon oxide on wire anode of positive corona discharge," *Jpn. J. Appl. Phys.* **27**, 1381–1385 (1988).
21. K. Nashimoto, "Silicon oxide projections grown by negative corona discharge," *Jpn. J. Appl. Phys.* **27**, 892–898 (1988).
22. K. Nashimoto, "Effect of anode surface on growth of silicon oxide needles induced by positive corona discharge," *Jpn. J. Appl. Phys.* **27**, L1181–L1183 (1988).
23. K. Nashimoto, "Morphology and structure of silicon oxides grown on wire electrode by positive discharge," *J. Electrochem. Soc.* **136**, 2320–2327 (1989).
24. U. Kortshagen and B. G. Heil, "Kinetic two-dimensional modeling of inductively coupled plasmas based on a hybrid kinetic approach," *IEEE Transactions on Plasma Science* **27**, 1297–1309 (1999).
25. A. Sherman, *Chemical Vapor Deposition for Microelectronics: Principles, Technology, and Applications*, Noyes Publications, Park Ridge, NJ (1987).
26. W. H. Tao, M. A. Prelas, and H. K. Yasuda, "Spatial distribution of electron density and electron temperature in direct current glow discharge," *J. Vac. Sci. Technol. A* **14**, 2113–2121 (1996).
27. L. L. Alves, G. Gousset, and C. M. Ferreira, "Self-contained solution to the spatially inhomegeneous electron Boltzmann equation in a cylindrical plasma positive column," *Physical Review E* **55**, 890–906 (1997).
28. V. Guerra and J. Loureiro, "Electron and heavy particle kinetics in a low-pressure nitrogen glow discharge," *Plasma Sources Sci. Technol.* **6**, 362–372 (1997).
29. E. U. Landers, "Distribution of electrons and ions in a corona discharge," *Proc. IEE* **125**, 1069–1073 (1978).
30. Y. Takahashi, M. Yoshida, Y. Anma, S. Kobayashi, and M. Endo, "Thickness and luminosity distribution of positive corona sheath in air," *J. Phys. D: Appl. Phys.* **15**, 639–653 (1982).
31. I. A. Kossyi, A. Y. Kostinsky, A. A. Matveyev, and V. P. Silakkov, "Kinetic scheme of the nonequilibrium discharge in nitrogen–oxygen mixtures," *Plasma Sources Sci. Technol.* **1**, 207–220 (1992).
32. P. Cooperman, "A theory for space-charge-limited current with application to electrical precipitation," *Trans. Amer. Inst. Elec. Eng.* **79**(Part 1), 47–50 (1960).
33. G. Cooperman, "A new current–voltage relation for duct precipitators valid for low and high current densities," *IEEE Transactions on Industry Applications* **1A–17**, 236–239 (1981).
34. G. Leutert and B. Bohlen, "The spatial trend of electric field strength and space charge density in a plate-type electrostatic precipitator," *Staub-Reinhalt. Luft* (in English) **32**, 27–37 (1972).

35. J. R. McDonald, W. B. Smith, H. W. Spencer III, and L. E. Sparks, "A mathematical model for calculating electrical conditions in wire-duct electrostatic precipitation devices," *Journal of Applied Physics* **48**, 2231–2243 (1977).
36. H. J. White, *Industrial Electrostatic Precipitation*, Addison–Wesley Publishing Company, Inc., Massachusetts (1963).
37. E. Lami, F. Mattachini, I. Gallimberti, R. Turri and U. Tromboni, "A numerical procedure for computing the voltage-current characteristics in electrostatic precipitator configurations," *Journal of Electrostatics* **34**, 385–399 (1995).
38. J. H. Goo and J. W. Lee, "Stochastic simulation of particle charging and collection characteristics for a wire-plate electrostatic precipitator of short length," *J. Aerosol Sci.* **28**, 875–893 (1997).
39. K. Adamiak, "Simulation of corona in wire-duct electrostatic precipitator by means of the boundary element method," *IEEE Transactions on Industry Applications* **30**, 381–386 (1994).
40. M. P. Sarma and W. Janischewskyj, "DC corona on smooth conductors in air," *Proc. IEE* **116**, 161–166 (1969).
41. R. W. Evans and I. I. Inculet, "The radius of the visible ionization layer for positive and negative coronas," *IEEE Trans. Ind. Appl.* **IA–14**, 523–525 (1978).
42. L. G. H. Huxley and R. W. Crompton, *The Diffusion and Drift of Electrons in Gases*, John Wiley and Sons, New York (1974).
43. M. A. Harrison and R. Geballe, "Simultaneous measurement of ionization and attachment coefficients," *Physical Review* **91**, 1–7 (1953).
44. S. Badaloni and I. Gallimberti, *Basic Data of Air Discharge*, Universita Di Padova, Padova, Italy (1972).
45. H. Ryzko, "Drift velocity of electrons and ions in dry and humid air and in water vapor," *Proc. Phys. Soc.* **85**, 1283–1295 (1965).
46. E. W. McDaniel and E. A. Mason, *The Mobility and Diffusion of Ions in Gases*, John Wiley and Sons, New York (1973).
47. R. Morrow, "The theory of positive glow corona," *J. Phys. D: Appl. Phys.* **30**, 3099–3114 (1997).
48. G. N. Aleksandrov, "Physical conditions for the formation of an ac corona discharge," *Soviet Phys. Tech. Phys.* 1714–1726 (1956).
49. R. Morrow and J. J. Lowke, "Streamer propagation in air," *J. Phys. D: Appl. Phys.* **30**, 614–627 (1997).
50. F. W. Peek, *Dielectric Phenomena in High-Voltage Engineering*, 3rd ed., McGraw-Hill, New York (1929).
51. I. P. Shkarofsky, T. W. Johnston, and M. P. Bachyanski, *The Particle Kinetics of Plasmas*, Addison–Wesley Publishing Company, Massachusetts (1966).
52. U. Kortshagen, C. Busch, and L. D. Tsendin, "On simplifying approaches to the solution of the Boltzmann equation in spatially inhomogeneous plasmas," *Plasma Sources Sci. Technol.* **5**, 1–17 (1996).
53. U. Kortshagen, *Boltzmann Solver for a* 0-*D Time-Dependent BE*, Minneapolis, MN (2000).
54. A. V. Phelps and L. C. Pitchford, "Anisotropic scattering of electrons by N_2 and its effect on electron transport," *Physical Review A* **31**, 2932–2949 (1985).
55. S. A. Lawton and A. V. Phelps, "Excitation of the $b\,^1\Sigma_g^+$ state of O_2 by low energy electrons," *J. Chem. Phys.* **69**, 1055–1068 (1978).
56. P. C. Cosby, "Electron-impact dissociation of oxygen," *J. Chem. Phys.* **98**, 9560–9569 (1993).